Field-induced barrier transparency of Bloch waves in tight-binding lattices

Stefano Longhi
Dipartimento di Fisica, Politecnico di Milano, Piazza L. da Vinci 32, I-20133 Milano, Italy

A rectangular potential barrier for a Bloch particle in a tight-binding lattice is shown to become fully transparent by the application of a strong ac field with appropriate amplitude and frequency. Such a curious phenomenon bears some connection with the field-induced barrier transparency effect known for freely-moving particles scattered by an ac-driven rectangular barrier; however, for a Bloch particle transparency is not related to a resonant tunnneling process across the cycle-averaged oscillating potential barrier, as for the freely-moving quantum particle. The phenomenon of field-induced transparency is specifically discussed here for photonic transport in waveguide arrays and demonstrated by full numerical simulations of the paraxial (Schrödinger) wave equation beyond the tight-binding approximation.

PACS numbers: 73.23.-b,73.40.Gk,42.82.Et, 78.67.Hc

I. INTRODUCTION

Coherent control of electronic, photonic or matter wave transport in driven semiconductor superlattices, quantum dots, waveguide arrays and optical lattices has received a great and continuous interest over the past two decades [1–4], stimulating a wide number of experimental and theoretical investigations in different physical systems [5–10]. Examples of coherent control by the application of ac fields include, among others, the coherent destruction of tunneling between two wells in a bistable potential [6] and the suppression of quantum diffusion and dynamic localization in tight-binding lattices [5]. Such phenomena have been demonstrated in a series of recent experiments [8–10], mainly based on transport of light waves or cold atoms in waveguide arrays or optical lattices, where dephasing and many-body effects can be neglected. Other interesting phenomena occur in the tunneling and scattering processes of ac-driven free particles across potential wells or barriers [11–14]. In particular, a freely-moving quantum particle can be resonantly transmitted across a periodically-driven rectangular potential barrier, in spite the probability of tunneling through the static potential barrier is almost zero [11, 12]. This phenomenon, originally predicted for quantum tunneling and referred to as field-induced barrier transparency [11, 12], is rather generic and can be similarly observed for optical tunneling at modulated dielectric interfaces [15]. In the accelerated (Kramers-Henneberger) reference frame, the ac-driven barrier behaves like a periodically-shaken potential barrier [11, 14]. At high oscillation frequencies, the oscillating rectangular barrier can be replaced at leading order by its cycle-averaged (static) barrier, whose profile shows a characteristic double-hump shape that sustains metastable states. Thus resonant transmission of the incident particles across the ac-driven barrier observed at certain below-barrier energies can be simply explained as a resonant tunneling process, similar to e.g. the Ramsauer-Townsend effect, the resonant electronic tunneling across a double-barrier structure, or the resonant light transmission of light in a Fabry-Perot optical cavity. In this work we consider the coherent motion of a Bloch particle in a tight-binding lattice with a strong impenetrable rectangular potential barrier, and demonstrate that the application of an ac field with appropriate amplitude and frequency can make the potential barrier fully transparent. This phenomenon, which can be again referred to as field-induced barrier transparency for Bloch particles in analogy to its counterpart for free particles, has however a very different origin. In particular, barrier transparency is observed for incident Bloch waves at *any* allowed energy in the band, i.e. it is not related to resonant tunneling of the cycled-averaged potential as in the free particle case. Here we investigate the phenomenon of field-induced barrier transparency of Bloch waves by considering photonic transport in periodically-curved waveguide lattices [4, 9], however the present analysis is rather generic to coherent transport in driven tight-binding lattices and could be therefore of interest to other physical set ups, such as to cold atoms or Bose-Einstein condensates in accelerated optical lattices [10].

The paper is organized as follows. In Sec.II, the basic model is described with specific reference to light transport in photonic lattices, and a theoretical analysis of field-induced barrier transparency in ac-driven tight-binding lattices is presented. In Sec.III the theoretical predictions obtained in the high-frequency regime are confirmed by direct numerical simulations, based on both the time-periodic coupled-mode equations of the driven tight-binding lattice and the Schrödinger wave equation with a one-dimensional potential. Deviations from the predictions based on the averaged lattice model in the high frequency modulation limit, such as a shift of the resonant curves, are briefly discussed. Finally, in Sec.IV the main conclusions are outlined.

II. FIELD-INDUCED BARRIER-TRANSPARENCY IN AC-DRIVEN TIGHT-BINDING LATTICES: THEORETICAL ANALYSIS

The starting point of our analysis is provided by a standard model of light transport in a one-dimensional array of tunneling-coupled optical waveguides with a periodically-curved optical axis [4, 9]. In the waveguide reference frame, light transport is described by the following Schrödinger-type wave equation for the electric field envelope $\phi(x,z)$ (see, for instance, [4, 16])

$$i\lambda\frac{\partial\phi}{\partial z}=-\frac{\lambda^2}{2n_s}\frac{\partial^2\phi}{\partial x^2}+V(x)\phi-F(z)x\phi\equiv\mathcal{H}_0\phi-F(z)x\phi, \tag{1}$$

where $\lambda=\lambda/(2\pi)$ is the reduced wavelength of light waves, n_s the substrate refractive index, x and z are the transverse and the longitudinal spatial coordinates, respectively, and $V(x)$ is the optical potential, which is related to the refractive index profile of the straight array by the simple relation $V(x)\simeq n_s-n(x)$. The last term on the right hand side of Eq.(1) is a fictitious refractive index gradient arising from axis bending and with a z-varying slope given by $F(z)=-n_s\ddot{x}_0(z)$, where $x_0(z)$ is the axis bending profile and the dot indicates the derivatives with respect to z [4]. In its present form, the paraxial wave equation (1) is formally equivalent to the Schrödinger equation describing the dynamics of a quantum particle of mass n_s in the potential $V(x)$ driven by a time-dependent external force $F(z)$, provided that the spatial z variable in the optical system is replaced by the temporal variable in the quantum problem, and the photon wavelength λ is replaced by the Panck's constant. The potential V is given by the superposition of the periodic and barrier potentials, i.e. $V(x)=V_p(x)+V_b(x)$, where $V_p(x+a)=V_p(x)$ is the periodic potential describing a homogeneous array of equally-spaced wells, and $V_b(x)$ is the barrier potential, which is assumed to describe a rectangular barrier of height V_0 and width $L\gg a$ [see Fig.1(a)]. The role of the barrier potential is to introduce a step, of height V_0, into a finite number of wells in the lattice, say from the waveguide $n=0$ to the waveguide $n=N$, as shown in Fig.1(a). The potential height V_0 is typically assumed to be much larger than the width of the lowest energy band of the array, yet smaller than the gap between the first and second lattice bands, as shown as an example in Fig.1(c). In this way, in the absence of the ac driving force any Bloch wave packet, belonging to the lowest band of the lattice and traveling along the lattice, is reflected from the potential barrier [see Fig.1(c)]. To study the role of the ac driving force and the possibility to make the barrier transparent, let us introduce the nearest-neighboring tight-binding approximation and let us assume that the lattice is mostly excited in its lowest-order Bloch band. Such conditions are satisfied, for example, by considering an array of weakly-coupled waveguides which is initially excited by a broad beam tilted at an angle smaller than the Bragg angle

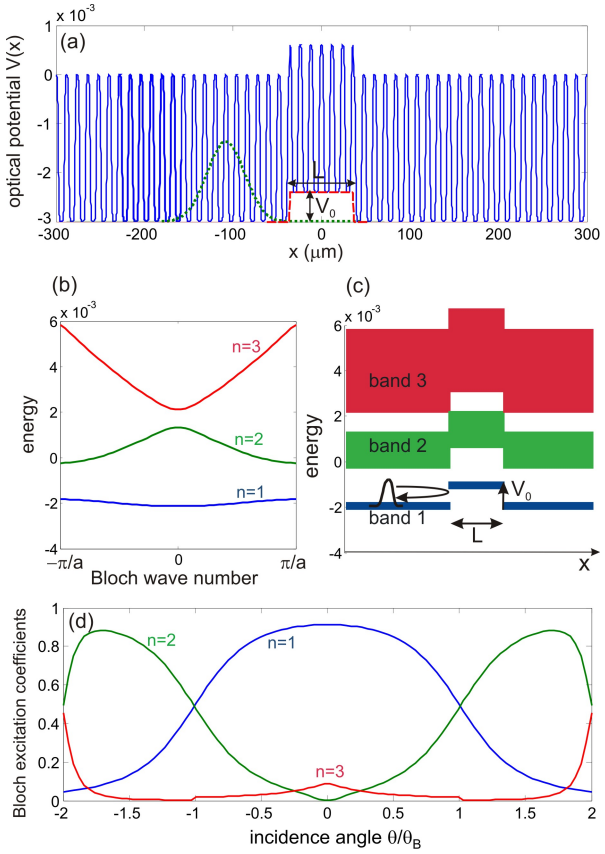

FIG. 1. (a) Behavior of the optical potential $V(x)=n_s-n(x)$ (solid curve) of a one-dimensional lattice with a barrier, composed by the superposition of the periodic optical potential (lattice period a) and of the rectangular barrier potential (height V_0, width L, represented by the dashed curve in the figure). The dotted curve in the figure is the intensity profile of the incident Gaussian wave packet in the numerical simulations of Sec.III.B. (b) Band diagram (three lower-order bands) of the periodic optical potential. The energy in the vertical axis is defined as the eigenvalue of the Hamiltonian $\mathcal{H}_0$ of the periodic potential entering in Eq.(1). (c) Space-energy band diagram of the lattice with the rectangular barrier. The height V_0 of the barrier is larger than the bandwidth 4Δ of the lowest lattice band, but smaller than the gap separating the first two bands. (d) Behavior of the Bloch excitation coefficients versus incidence angle θ of a plane wave, normalized to the Bragg angle $\theta_B=\lambda/(2a)$.

$\theta_B=\lambda/(2a)$ [9, 16]. Under such assumptions, from Eq. (1) the following coupled-mode equations can be derived [4, 9]

$$i\dot{c}_n=-\Delta(c_{n+1}+c_{n-1})-f(z)nc_n+\sigma\rho_n c_n \tag{2}$$

for the amplitudes c_n of the field trapped in the individual waveguides, where $\Delta>0$ is the coupling constant between adjacent waveguides,

$$f(z)\equiv\frac{a}{\lambda}F(z)=-\frac{an_s}{\lambda}\ddot{x}_0(z) \tag{3}$$

is the normalized forcing,

$$\sigma \equiv \frac{V_0}{\lambda}, \tag{4}$$

and

$$\rho_n \begin{cases} 1 & \text{for } 0 \le n \le N \\ 0 & \text{otherwise .} \end{cases} \tag{5}$$

To study field-induced barrier transparency, it is worth introducing, in place of c_n, the amplitudes a_n defined by the relations

$$a_n = c_n \exp\left[-in\int_0^z d\xi f(\xi) + i\sigma\rho_n z\right], \tag{6}$$

so that Eqs.(2) take the form

$$i\dot{a}_n = -\Delta_n(z)a_{n+1} - \Delta^*_{n-1}(z)a_{n-1} \tag{7}$$

where we have set

$$\Delta_n(z) = \Delta \exp\left[i\int_0^z d\xi f(\xi) + i\sigma(\rho_n - \rho_{n+1})\right]. \tag{8}$$

Let us now assume a sinusoidal bending of waveguide axis with spatial frequency $\omega = 2\pi/\Lambda$ and amplitude A, i.e.

$$x_0(z) = A\cos(2\pi z/\Lambda), \tag{9}$$

so that

$$f(z) = f_0\cos(2\pi z/\Lambda), \tag{10}$$

where

$$f_0 = \frac{4\pi^2 a n_s A}{\Lambda^2 \lambda}. \tag{11}$$

Let us also assume that:
(i) the barrier height V_0 and the quanta of modulation $\lambda\omega$ are much larger than the width $4\lambda\Delta$ of the tight-binding energy band;
(ii) the modulation frequency is chosen such that the resonant condition

$$l\omega = \sigma = \frac{V_0}{\lambda} \tag{12}$$

is satisfied for some (small) integer l (typically $l = 1$ or $l = 2$). In the high-modulation frequency limit [assumption (i)], at first order in a multiple-scale asymptotic analysis of Eqs.(7) the spatial evolution of the amplitudes a_n is dominated by the cycle-average coupling rates $\bar{\Delta}_n = (1/\Lambda)\int_0^\Lambda dz\Delta_n(z)$ (see, for instance, [17]), i.e. one has

$$i\dot{a}_n \simeq -\bar{\Delta}_n a_{n+1} - \bar{\Delta}^*_{n-1}a_{n-1}. \tag{13}$$

Taking into account that $\exp[i\Gamma\sin(\omega z)] = \sum_n J_n(\Gamma)\exp(in\omega z)$ and using Eqs.(5) and (10), from Eq.(8) it readily follows that

$$\bar{\Delta}_n = \begin{cases} \Delta J_0(\Gamma) & \text{for } n \ne -1, N \\ \Delta J_l(\Gamma) & \text{for } n = -1 \\ (-1)^l \Delta J_l(\Gamma) & \text{for } n = N \end{cases} \tag{14}$$

where we have set

$$\Gamma \equiv \frac{f_0}{\omega} = \frac{2\pi a n_s A}{\lambda\Lambda}. \tag{15}$$

Equations (13) thus describe light transport in an effective lattice with two defects in the coupling rates at lattice sites $n = -1$ and $n = N$. However, if the amplitude A of modulation is tuned such that

$$J_0(\Gamma) = \pm J_l(\Gamma), \tag{16}$$

the effective lattice is homogeneous (i.e. defect-free), and thus any Bloch wave packet propagates in the lattice without being reflected [18]. That is, if the modulation frequency and amplitude are tuned to satisfy the conditions (12) and (16), the effect of the ac driving is to make the barrier V_b fully transparent for Bloch wave packets belonging to the lowest energy band.

III. NUMERICAL SIMULATIONS

In this section we confirm, by direct numerical simulations of both the tight-binding equations (2) and the full wave equation (1), the field-induced barrier transparency phenomenon predicted in the previous section in the high-frequency modulation regime.

A. Tight-binding lattice model

Let us first consider beam reflection and transmission in the tight-binding lattice model described by the coupled-mode equations (2) with periodic coefficients. Equations (2) have been numerically integrated using an accurate fourth-order variable-step Runge-Kutta methods with absorbing boundary conditions. As an example, Figs.2(a-d) (upper panels) show the numerically-computed evolution of lattice site occupation probabilities $|c_n(z)|^2$ for $\sigma/\Delta = 4$, $N = 6$, $\omega = \sigma$ and for a few increasing values of the modulation amplitude, measured by the dimensionless parameter $\Gamma = f_0/\omega$. For comparison, the lower panels in Figs.2(a-d) show the corresponding evolution of occupation probabilities as obtained by integration of the averaged effective lattice equations [Eqs.(13) and (14)], valid in the high modulation frequency limit. The array is initially excited by a Gaussian distribution $c_n(0) = \exp[-(n-n_0)^2/w^2]\exp(iqn)$ with mean position $n_0 = -26$, width $w = 4$ and momentum $q = \pi/2$ (corresponding to the largest cycle-averaged group velocity far from the barrier). Note that at $\Gamma = 1.435$, at which the condition (16) is satisfied for $l = 1$, the wave packet is not reflected, and the barrier appears to be fully transparent [see Fig.2(c)]. In the simulations shown in Fig.2, the ratio $\omega/\Delta = 4$ is large enough to ensure the validity of the averaged equations (13), at least at first-order approximation. In fact, a more careful comparison of the results obtained from the original coupled-mode equations with periodic coefficients [Eqs.(2) or (7)]

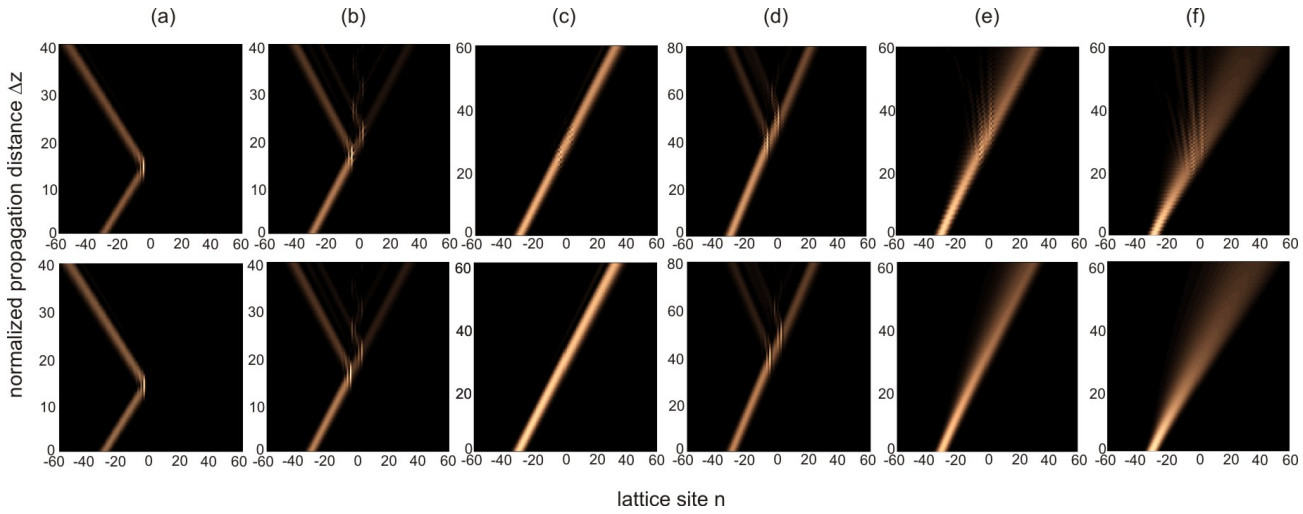

FIG. 2. Beam evolution (snapshots of lattice site intensities $|c_n(z)|^2$) for an initial Gaussian wave packet distribution with transverse momentum q as obtained by numerical simulations of the coupled-mode equations (2) (upper panels) and by the averaged equations (17) (lower panels) for $\sigma/\Delta = 4$ and $\omega = \sigma$. In (a-d), the initial transverse beam momentum is $q = \pi/2$, in (e) $q = \pi/3$, whereas in (f) $q = \pi/4$. In (a) $\Gamma = 0$ (non-modulated lattice), in (b) $\Gamma = 0.8$, in (c),(e),(f) $\Gamma = 1.435$ (transparency condition), in (d) $\Gamma = 1.8$.

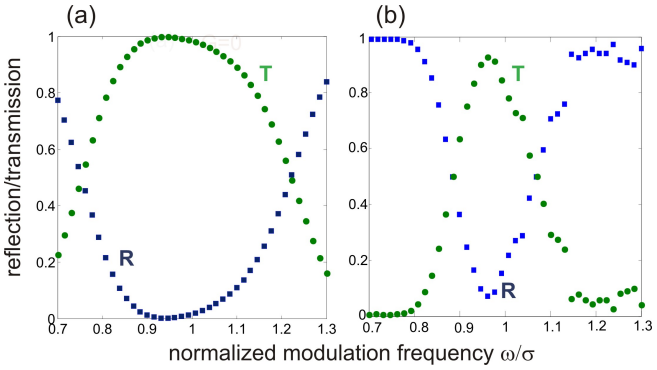

FIG. 3. Behavior of the power reflection (R) and transmission (T) coefficients of a Gaussian wave packet at the first barrier discontinuity near the first transparency resonance $\omega = \sigma$ numerically computed (a) using the tight-binding model (2), and (b) the full wave equation (1). Parameter values in the two cases are given in the text.

and the averaged equations (13) shows some slight discrepancies, which basically arise from neglecting higher-order terms in the asymptotic analysis of Eqs.(7) (for more details see, for instance, [17]). In particular, according to the average model (13), transparency should be observed regardless of the initial value of wave packet momentum q, i.e. of its mean energy; however, numerical simulations of the original (periodic) coupled-mode equations (2) show that some reflected light is observed at the barrier when the initial wave packet momentum q (i.e., its mean group group velocity) is reduced. This is shown, as an example, in Figs.2(e) and (f), where the evolution of lattice site occupation probabilities are depicted for the same initial Gaussian wave packet of Fig.2(c) (i.e. at the transparency condition), but with an initial momentum lowered to $q = \pi/3$ [Fig.2(e)] and $q = \pi/4$ [Fig.2(f)]. Another difference between the average and periodic coupled-mode equations can be seen by computing the first resonance curve of the transparency process, depicted in Fig.3(a). The figure shows the behavior of the power reflection R and transmission T coefficients versus ω (near the first resonance $\omega \sim \sigma = V_0/\lambda$) for the same initial Gaussian wave packet with momentum $q = \pi/2$, as obtained by numerical integration of Eqs.(2). For the sake of simplicity, the coefficients R and T have been computed by considering the first potential step solely of the barrier, so that multiple reflections that would arise in the presence of the two potential discontinuities of the rectangular barrier [see, for example, Fig.2(b)] are avoided . For each modulation frequency ω, the modulation amplitude A was correspondingly varied such that the ratio $\Gamma = f_0/\omega$ [see Eq.(15)] remains constant and equal to 1.435, at which the condition (16) is satisfied. Note that, the condition of exact transparency ($R = 0$) is attained at the ratio $\omega/\sigma \simeq 0.95$, which is slightly smaller than 1, as expected from the averaged model [Eq.(12) with $l = 1$]. As discussed above, the validity of the averaged model becomes more accurate, and the agreement between the averaged and original (periodic) coupled mode equations closer, as the ratio $\sim \sigma/\Delta$ of barrier height and width of tight-binding energy band is increased.

B. Full-wave equation

We checked the validity of the tight-binding lattice analysis and the onset of field-induced barrier trans-

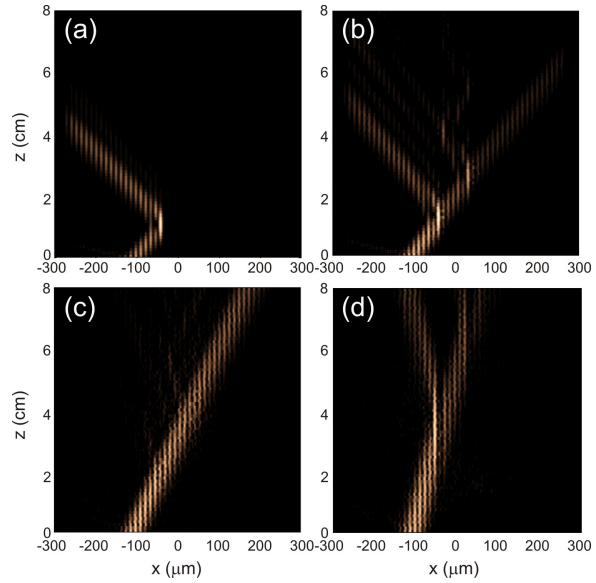

FIG. 4. Beam intensity evolution (snapshot of $|\phi(x,z)|^2$) of an initial Gaussian beam along the periodically-curved waveguide array of Fig.1(a) for increasing values of the modulation amplitude [measured by the parameter Γ, given by Eq.(15)]: (a) $\Gamma = 0$ (straight array); (b) $\Gamma = 0.8$, (c) $\Gamma = 1.435$ (transparency condition), and (d) $\Gamma = 1.8$. In all the simulations, the input Gaussian beam is tilted at the angle $\theta = \theta_B/2$, and the modulation frequency is $\omega = 0.98\sigma$.

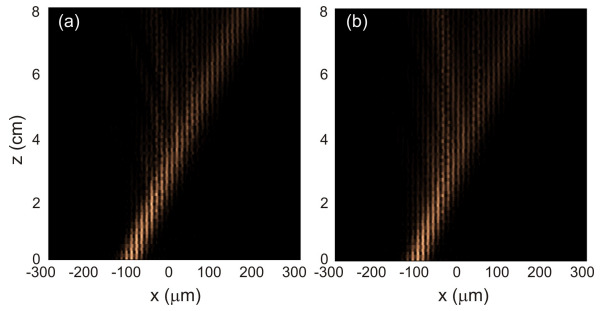

FIG. 5. Same as Fig.4, but for an initial Gaussian beam with $\Gamma = 1.435$, $\omega = 0.98\sigma$ and tilt angle (a) $\theta = \theta_B/3$, and (b) $\theta = \theta_B/4$.

parency in photonic waveguide arrays by direct numerical simulations of the paraxial wave equation (1) using standard pseudospectral methods. The optical potential $V(x) = n_s - n(x)$ of the lattice used in numerical simulations is shown in Fig. 1(a) and corresponds to a typical effective index profile of Lithium-Niobate waveguide arrays, fabricated by the proton-exchange technique and probed at $\lambda = 1.44$ μm wavelength (see, for instance, the experiment reported in Ref.[16]). The refractive index profile $n_w(x)$ of each waveguide in the array is taken to be given by [16]

$$n_w(x) = \Delta n \frac{\mathrm{erf}[(x+w_g)/D_x] - \mathrm{erf}[(x-w_g)/D_x]}{2\mathrm{erf}(w_g/D_x)} \quad (17)$$

where $w_g = 3.5$ μm is the channel width, $D_x = 1$ μm the diffusion length, and $\Delta n = 0.003$ the peak index change. The waveguide spacing (lattice period) is $a = 12$ μm, and the substrate refractive index at the probing wavelength is $n_s = 2.1381$. The band structure of the lattice, numerically computed by a standard plane-wave expansion method, is shown in Fig.1(b). From the width of the lowest order (tight-binding) lattice band, a coupling rate $\Delta \simeq 3.25$ cm^{-1} can be estimated between adjacent waveguides. When the lattice is excited by a broad wave packet, tilted at an angle θ, it generally breaks up into the superposition of different wave packets, belonging to the various lattice bands and refracting at different angles (see, for instance, [16, 19]). The fractional excitations of the different lattice bands are given by the Bloch-wave excitation coefficients C_n, defined as in Ref.[19]. Figure 1(d) shows the numerically-computed behavior of $C_n(\theta)$ for the various lattice bands of the periodic part of the optical potential of Fig.1(a) versus the tilt angle θ of the incident beam, in units of the Bragg angle $\theta_B = \lambda/(2a)$. As one can see, for broad input beams tilted at an angle θ smaller than half of the Bragg angle, the lowest-order lattice band is mainly excited, which indicates that in this case the tight-binding model of Sec.II can be safely applied. The barrier height used in the numerical simulations is $V_0 = \Delta n/5 = 6 \times 10^{-4}$, whereas its width is $L = 72$ μm. A schematic of the space-dependent band diagram of the lattice, shown in Fig.1(c), clearly indicates that, in the absence of the external ac field, the barrier is impenetrable and any Bloch wave packet, incident onto the barrier, is reflected. This is shown, as an example, in Fig.4(a), where the numerically-computed evolution of the field intensity $|\phi(x,z)|^2$ along the non-modulated lattice is depicted by assuming, as an initial condition, the tilted Gaussian beam $\phi(x,0) = \exp[-(x+x_0)^2/w^2]\exp(2\pi i\theta x/\lambda)$ with spot size $w = 30$ μm, offset $x_0 = 108$ μm [see the dotted curve in Fig.1(a)] and tilt angle $\theta = \theta_B/2 \simeq 1.719^o$. Let us now introduce a sinusoidal modulation of the axis bending $x_0(z)$ at a spatial frequency $\omega = 2\pi/\Lambda$ close to the first resonance [$l = 1$ in Eq.(12)], which corresponds to a spatial modulation period $\Lambda = 2.45$ mm. Note that the ratio between modulation frequency ω and coupling rate Δ of waveguides turns out to be ~ 7.9, i.e. the high frequency modulation condition is well satisfied. Figures 4(b-d) show the evolution of the same Gaussian wave packet as in Fig.4(a) but in the periodically-curved waveguide array for increasing values of the modulation amplitude A, measured by the dimensionless parameter Γ given by Eq.(15). Note that the cycle-averaged transverse group velocity of the wave packet, far from the barrier region and at the tilting angle $\theta = \theta_B/2$, is equal to $v_g = 2\Delta a|J_0(\Gamma)|$, and thus decreases as Γ is increased from zero [Fig.4(a)] to $\Gamma = 1.8$ [Fig.4(d)]. As the modulation is increased, the Gaussian wave packet is less and less reflected from the barrier, till a nearly reflectionless regime, corresponding to full barrier transparency, is attained when the transparency condition (16) is reached

[see Fig.4(c)]. Barrier transparency is observed at different values of the initial tilt angle θ (i.e. initial wave packet momentum), expect for small tilt angles at which the wave packet shows a more complex dynamics at the barrier crossing (see Fig.5). This behavior, already noticed in Sec.II in the framework of the tight-binding analysis, is mainly ascribable to a discrepancy between the average model [Eq.(13)] and the original coupled-mode equations with periodic coefficients [Eqs.(2) or (7)]. A slight discrepancy can be also seen when computing the resonance curve of the field-induced barrier transparency process using the full wave equation (1), similarly to what already noticed within the tight-binding model [see Fig.3(a)]. In Fig.3(b), the numerically-computed power reflection (R) and transmission (T) coefficients versus ω (near the first resonance $\omega \sim \sigma = V_0/\lambda$) are depicted for the Gaussian wave packet of Fig.4. Like for the resonance curve computed using the tight-binding model [Fig.3(a)], the coefficients R and T have been calculated by considering the first potential step solely of the barrier, and for each modulation frequency ω the modulation amplitude A was correspondingly varied such that $\Gamma = f_0/\omega = 1.435$. Note that, as in Fig.3(a), the resonance frequency turns out to be slightly smaller than the theoretical value σ predicted by the averaged model.

As a concluding remark, it is important to stress that, as compared to the phenomenon of field-induced barrier transparency for a freely-moving quantum particle [11] in which particle transmission occurs solely at special values of initial momentum (energy) that match the metastable states of the cycle-average potential barrier, the phenomenon of barrier transparency for Bloch wave packets predicted in this work is relatively insensitive to the initial wave packet momentum and can not thus be ascribed to a resonant tunneling phenomenon as for the free particle. However, as opposed to the case of Ref.[11], where the frequency and amplitude of the ac field may take relatively arbitrary values [20], in our system the modulation frequency as well as the modulation amplitude should satisfy certain resonance conditions, namely Eqs.(12) and (16).

IV. CONCLUSIONS

In this work it has been theoretically shown that a rectangular potential barrier for a Bloch particle in a tight-binding lattice can be made fully transparent by the application of a strong ac field with appropriate amplitude and frequency. As this phenomenon bears some connection with the field-induced barrier transparency phenomenon previously predicted for freely-moving quantum particles scattered by an ac-driven potential barrier [11, 12], the transparency effect for the Bloch particle has a rather different physical origin, as discussed in this work. In particular, in the high-frequency limit transparency is attained independently of the energy of the Bloch wave packet, and therefore particle transmission across the barrier can not be explained as a resonant tunneling process across the cycle-averaged potential, as for a freely moving particle [11]. This phenomenon could be experimentally observed in periodically-curved waveguide arrays, where light transport along the lattice mimics the coherent temporal evolution of a Bloch particle with an external ac driving field [9]. Numerical simulations based on the paraxial (Schrödinger) wave equation have also shown that the phenomenon of field-induced barrier transparency persists beyond the tight-binding approximation, provided that the lattice is initially excited by a broad beam tilted at an angle smaller than the Bragg angle.

ACKNOWLEDGMENTS

This work was supported by the Italian MIUR (Grant No. PRIN-20082YCAAK, "Analogie ottico-quantistiche in strutture fotoniche a guida d'onda").

[1] M. Grifoni and P. Hänggi, Phys. Rep. **304**, 229 (1998); S. Kohler, J. Lehmann, and P. Hänggi, Phys. Rep. **406**, 379 (2005).

[2] M. Glück, A. R. Kolovsky, and H. J. Korsch, Phys. Rep. 366, 103 (2002).

[3] T. Dittrich, P. Hänggi, G.-L. Ingold, B. Kramer, G. Schön, and W. Zwerger, *Quantum transport and dissipation* (Wiley-VCH, New York, 1998).

[4] S. Longhi, Laser Photon. Rev. **3**, 243 (2009).

[5] D.H. Dunlap and V.M. Kenkre, Phys. Rev. B **34**, 3625 (1986); M. Holthaus, Phys. Rev. Lett. **69**, 351 (1992); M. M. Dignam and C. M. de Sterke, Phys. Rev. Lett. **88**, 046806 (2002).

[6] F. Grossmann, T. Dittrich, P. Jung, and P. Hänggi, Phys. Rev. Lett. **67**, 516 (1991); F. Grossmann, P. Jung, T. Dittrich, and P. Hänggi, Z. Phys. B: Condens. Matter **84**, 315 (1991).

[7] M. Holthaus, G.H. Ristow, and D.W. Hone, Phys. Rev. Lett. **75**, 3914 (1995); S. Raghavan, V. M. Kenkre, D. H. Dunlap, A. R. Bishop, and M. I. Salkola, Phys. Rev. A **54**, R1781 (1996); J. Karczmarek, M. Stott, and M. Ivanov, Phys. Rev. A **60**, R4225 (1999); J.T. York, R.D. Coalson, and Y. Dahnovsky, Phys. Rev. B **65**, 235321 (2002); M.V. Fistul, A.E. Miroshnichenko, and S. Flach, Phys. Rev. B **68**, 153107 (2003); C.E. Creffield, Phys. Rev. B **67**, 165301 (2003); J.M. Villas-Boas, S.E. Ulloa, and N. Studart, Phys. Rev. B **70**, 041302(R) (2004); K. Saito and Y. Kayanuma, Phys. Rev. B **70**, 201304(R) (2004); C.E. Creffield and G. Platero, Phys. Rev. B **69**, 165312 (2004); A. Eckardt, C. Weiss, and M. Holthaus, Phys. Rev. Lett. **95**, 260404 (2005); C.E. Creffield and T. S. Monteiro. Phys. Rev. Lett. **96**, 210403 (2006); C.

Weiss, Phys. Rev. B **73**, 054301 (2006); C.E. Creffield, Phys. Rev. Lett. **99**, 110501 (2007); J. Gong, D. Poletti, and P. Hänggi, Phys. Rev. A **75**, 033602 (2007); C.E. Creffield, J. Phys.: Conf. Ser. **150**, 032017 (2009); G. Lu, W. Hai, and H. Zhong, Phys. Rev. A **80**, 013411 (2009); D. Zueco, F. Galve, S. Kohler, and P. Hänggi Phys. Rev. A **80**, 042303 (2009); J. Abdullaev, D. Poletti, E.A. Ostrovskaya, and Y.S. Kivshar, Phys. Rev. Lett. **105**, 090401 (2010).

[8] G. Della Valle, M. Ornigotti, E. Cianci, V. Foglietti, P. Laporta, and S. Longhi, Phys. Rev. Lett. **98**, 263601 (2007); E. Kierig, U. Schnorrberger, A. Schietinger, J. Tomkovic, and M. K. Oberthaler, Phys. Rev. Lett. **100**, 190405 (2008).

[9] S. Longhi, M. Marangoni, M. Lobino, R. Ramponi, P. Laporta, E. Cianci, and V. Foglietti, Phys. Rev. Lett. **96**, 243901 (2006); R. Iyer, J. Aitchison, J. Wan, M. Dignam, and M. de Sterke, Opt. Express **15**, 3212 (2007); A. Szameit, I. L. Garanovich, M. Heinrich, A. A. Sukhorukov, F. Dreisow, T. Pertsch, S. Nolte, A. Tünnermann, and Y. S. Kivshar, Nature Phys. **5**, 271 (2009); A. Joushaghani, R. Iyer, J.K.S. Poon, J.S. Aitchison, C.M. de Sterke, J. Wan, and M.M. Dignam, Phys. Rev. Lett. **103**, 143903 (2009); A. Szameit, I.L. Garanovich, M. Heinrich, A.A. Sukhorukov, F. Dreisow, T. Pertsch, S. Nolte, A. Tünnermann, S. Longhi, and Y.S. Kivshar, Phys. Rev. Lett. **104**, 223903 (2010).

[10] K.W. Madison, M. C. Fischer, R. B. Diener, Q. Niu, and M. G. Raizen, Phys. Rev. Lett. **81**, 5093 (1998); H. Lignier, C. Sias, D. Ciampini, Y. Singh, A. Zenesini, O. Morsch, and E. Arimondo, Phys. Rev. Lett. **99**, 220403 (2007); A. Eckardt, M. Holthaus, H. Lignier, A. Zenesini, D. Ciampini, O. Morsch, and E. Arimondo, Phys. Rev. A **79**, 013611 (2009); A. Zenesini, H. Lignier,D. Ciampini, O. Morsch, and E. Arimondo, Phys. Rev. Lett. **102**, 100403 (2009); O. Morsch, D. Ciampini, and E. Arimondo, Europhys. News **41**, 21 (2010).

[11] I. Vorobeichik1, R. Lefebvre, and N. Moiseyev, Europhys. Lett. **41**, 111 (1998); I. Vorobeichik and N. Moiseyev, J. Phys. B **31**, 645 (1998); I. Vorobeichik and N. Moiseyev, Phys. Rev. A **59**, 1699 (1999).

[12] M.L. Chiofalo, M. Artoni, and G.C. La Rocca, New Jour. Phys. **5**, 78 (2003); D. Embriaco, M.L. Chiofalo, M. Artoni, and G.L. La Rocca, J. Opt. B: Quant. Sem. Opt. **7**, S59 (2005); F.Kh. Abdullaev and J. Garnier, Phys. Rev. A **75**, 033603 (2007).

[13] G.A. Luna-Acosta, G. Orellana-Rivadeneyra, A. Mendoza- Galvan, and C. Jung, Chaos, Solitons Fractals **12**, 349 (2001); K. Takahashi and K. S. Ikeda, Ann. Phys. (N.Y.) 283, 94 (2000).

[14] M. Henseler, T. Dittrich and K. Richter, Europhys. Lett. **49**, 289 (2000); M. Henseler, T. Dittrich, and K. Richter, Phys. Rev. E **64**, 046218 (2001).

[15] S. Longhi, Opt. Lett. **15**, 2781 (2005).

[16] S. Longhi, M. Lobino, M. Marangoni, R. Ramponi, P. Laporta, E. Cianci, and V. Foglietti, Phys. Rev. B **74**, 155116 (2006).

[17] S. Longhi, Phys. Rev. B **77**, 195326 (2008).

[18] It should be noted that, once Eq.(16) is satisfed, a change of the sign of the coupling rate between adjacent sites at $n = -1$ or $n = N$ can occur. However, such a sign change does not introduce reflection of a wave packet propagating in the lattice. In fact, by a suitable change of the phase of the amplitudes a_n, the lattice (13) with some sign changes in the coupling rates become fully equivalent to a homogeneous lattice with constant coupling rates between adjacent sites.

[19] A.A. Sukhorukov, D. Neshev, W. Krolikowski, and Y. S. Kivshar, Phys. Rev. Lett. **92**, 093901 (2004); R. Morandotti, D. Mandelik, Y. Silberberg, J. S. Aitchison, M. Sorel, D. N. Christodoulides, A. A. Sukhorukov, and Y. S. Kivshar, Opt. Lett. **29**, 2890 (2004); S. Longhi, Opt. Lett. **31**, 1857 (2006).

[20] The only condition on the modulation frequency is that its value should be large enough in order to ensure the validity of the average potential model. The modulation amplitude should be also large enough to ensure that the cycle-averaged potential barrier sustains some metastable states (see [11] for more details).